10th International Fall Workshop

VISION, MODELING, AND VISUALIZATION 2005

November 16 - 18, 2005

Erlangen, Germany

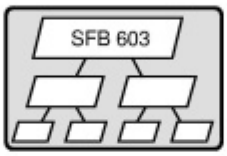

organized by

DFG Collaborative Research Center SFB 603
Model-based Analysis and Visualization of Complex Scenes and Sensor Data

in cooperation with

Gesellschaft für Informatik GI

European Association for Computer Graphics Eurographics

Deutsche Arbeitsgemeinschaft für Mustererkennung DAGM

Fraunhofer Institute for Integrated Circuits IIS-A

Marcus Prümmer, Jingfeng Han, Joachim Hornegger,
2D-3D Non-rigid Registration using Iterative Reconstruction.
In: Vision Modeling and Visualization, Workshop Vision Modeling and Visualization in Erlangen 2005, p. 187-194, ISBN: 3-89838-068-8

2D-3D Non-rigid Registration using Iterative Reconstruction

M. Prümmer, J. Han, J. Hornegger

University of Erlangen-Nuremberg, Germany,
Email: {pruemmer, jingfeng, hornegger}@informatik.uni-erlangen.de

Abstract

In this paper, we propose a novel intensity–based method that address non–rigid 2D-3D registration problem. This method allows non–rigid transformation for volumetric data to establish the proper alignment with a sparse number of 2D projections. The key issue of nonrigid 2D-3D registration is how to define the distance measure between 3D data and 2D projection. In this work, we use the idea that comes from algebraic reconstruction theory to handle this problem. We modify the Euler–Lagrange equation by introducing a new 3D force. This external force term is computed from the residual of the algebraic reconstruction procedures. It means that we integrate the algebraic reconstruction technique into the variational registration framework, so that the 3D displacement field is driven to minimize the "reconstruction distance" between volumetric data and those 2D projections. Experimental results are presented on both artificial phantom and a real 3D *Digital Subtraction Angiography* (DSA) data.

1 Introduction

The 2D-3D registration has great value in many medical applications. Volumetric CT are frequently used in clinical diagnosis and surgical planning. However, it is uncommon to acquire those 3D data as interventional imaging modalities. Typically, the intra–procedural data sets are presented in two–dimensional information, like X-ray fluoroscopes. Although these images lack the spatial details of volumetric data, they can be acquired in real time and with minor radiation exposure to patients. The goal of 2D-3D registration is to find the 3D transform that aligns reconstructed volumes with intra–interventional 2D images in order to make use of up–to–date information for surgical guidance and other interventions.

Many 2D-3D registration methods are proposed by literatures. According to the distance measure, these methods can be roughly classified into feature–based and intensity–based. Feature–based approaches make use of landmarks (fiducial or natural) or the other anatomical features to match images. For example, Gueziec et al. [1] use surface features to align CT volume with fluoroscopy X-ray. Feldmar et al. [2] presented a unified framework for 2D-3D registration of curves and surfaces. Hamadeh et al. [3] extended Feldmar's method by combining segmentation result of X-ray images. Intensity–based registration measure the similarity of intensity directly. Thus, no feature extraction is required and the whole registration procedure can be automatic. E.g., Weese et al. [4] presented an intensity–based method for 2D-3D registration. LaRose et al [5] investigate real time iterative X-ray/CT registration techniques. Zollei et al. [6] employ mutual information as similarity measure and stochastic gradient ascent approach as optimization procedure in 2D-3D registration problems. Yao et al. [7] proposed an affine 2D-3D registration method based on a statistical model.

Most of the prior work focused on parameterized transformation, such as rigid or affine transformation, i.e., the spatial transforms are defined by a set of parameters. However, in many clinic applications, it is more reasonable to describe the spatial transformations with a non–parameterized model, i.e., the *displacement field*. Our work is actually motivated by the limitation of nowadays methods. In this paper we propose a way that allows non–rigid transformation for volumetric data to establish the proper alignment with a sparse number of two–dimensional projections.

The key issue of nonrigid 2D-3D registration is how to define the distance measure between 3D data and 2D projection. In this work, we use the idea that comes from algebraic reconstruction theory to handle this problem. One distinguish viewpoint of this paper is that the 2D-3D registration problem

can be somehow regarded as in a certain "reconstruction" procedure, in which the volumetric data is the initial volume and the reference 2D images are used to further "reconstruct" the volume. However, instead of updating the intensity values of the floating volume as a common reconstruction procedure, we use the residual of the algebraic reconstruction to drive the registration equation to find the appropriate spatial transformation. It means that we integrate algebraic reconstruction technique into variational registration framework, so that the 3D displacement field is driven to minimize the "reconstruction distance" between volumetric data and those two–dimensional projections.

The paper is organized as following. Firstly, we briefly introduce the non–rigid registration method and the algebraic reconstruction. Then, we combine these two techniques in a uniform framework to handle the 2D-3D registration problem. Finally, we verify our approach via experiments on both phantom data and a real 3D reconstructed medical image with a synthetic deformation.

2 Mono–dimensional registration

In this section we briefly introduce the framework of the intensity–based nonrigid registration of same dimensional images. Here, two volumetric data are given, template volume $T(x)$ and reference volume $R(x)$. For simplification, the intensities of image data have been scaled into $]0,1[$. The mathematical description of mono–dimensional registration problem is to find a displacement field $u : \mathbb{R}^d \rightarrow \mathbb{R}^d$, such that

$$\mathcal{J}[u] := \mathcal{D}[R, T; u] + \alpha \mathcal{S}[u] = \min \qquad (1)$$

The *distance measure* $\mathcal{D}$ indicts the dissimilarity between two volumes. E.g., *sum of squared differences* (SSD) is one of the most popular distance measures for monomodal registration problems. It is defined as:

$$\mathcal{D}^{\mathrm{SSD}}[R, T; u] := \frac{1}{2} \int_{\Omega} \left(T(x - u(x)) - R(x)\right)^2 \, dx \qquad (2)$$

The *regularizer* $\mathcal{S}$ in Eq.(1) is added as the remedy for the arbitrary irregularity of transformation. Many regularizers have been proposed by literature [8]-[12]. Here we employ the *curvature regularizer*, which is defined as:

$$\mathcal{S}^{curv}[u] := \frac{1}{2} \sum_{l=1}^{d} \int_{\Omega} (\Delta u_l)^2 \, dx \qquad (3)$$

According the theory of variational calculus, the optimal $u(x)$ in (3) is characterized by the related Euler–Lagrange equation

$$f(x, u(x)) + \alpha \Delta^2 [u](x) = 0. \qquad (4)$$

$f(x, u(x))$ is called external force term, which is computed from the intensity of images after transformation. It drives the algorithm to search for the optimal displacement $u(x)$ that aligns images. Mathematically, $f(x, u(x))$ is the Gâteaux derivative of distance measure $\mathcal{D}$ in (1). For the SSD distance measure, the force can be computed as following,

$$f = D_u^I \cdot \nabla T(x - u(x)) \qquad (5)$$

Here $\nabla T(x - u(x))$ is the gradient vector field of transformed image. It contains the structure information of the underlying objects and determines the direction of the force term. $D_u^I = (R(x) - T(x - u(x)))$ is the substraction of two images' intensities. It can be understood as a signed distance between $[-1, 1]$. If two mono–modal images are to be aligned, this factor D_u^I will approach to 0 and the force will nearly vanish. An $\mathcal{O}(N \log N)$ numerical scheme for equation (4) was designed in [12].

The conventional mono–dimensional non–rigid registration techniques are not applicable in 2D-3D registration problem, because their distance measures (like SSD) fail to express the dissimilarities between 3D volume and 2D projections.

3 Nonrigid 2D-3D registration

The 2D-3D registration can be defined as following. We have the floating volume T and a number of 2D projections R^{ϕ}'s. Here $\phi = 0, ..., \Phi$ and Φ is the number of projections. Given the projection model, the task of nonrigid 2D-3D registration is to find the 3D displacement $u(x)$ that align the volume T to the 2D projections R^{ϕ}'s.

In order to solve 2D-3D registration under variational framework, we need to find a proper distance, let's say D_u^R, to take place the D_u^I in (5), which

describes the dissimilarity between the 2D-3D images. Such distance need to fulfill following criterion:

- D_u^R must be bounded.
- The value of D_u^R can indicate a signed distance between T and R^ϕ's.
- If the R^ϕ's are the projections of the T, $D_u^R = 0$.

In this paper we propose the *residuals* between 2D projections and 3D volume as this signed distance. The residuals terms are extensively used in the iterative reconstruction approaches, e.g., Cimmino's simultaneous projection method [17] or Censor and Gordon's component averaging algebraic reconstruction schemes [14]. Different algebraic reconstruction techniques (ART) have different residual weighting terms. But all the residuals satisfy previous three criterion of D_u^R. In the following, we introduce the relevant knowledge about algebraic reconstruction, then present the new 3D force term based on residuals and give the overall algorithm finally.

3.1 Algebraic Reconstruction Technique

For the ease of presentation we serialize T into a vector $\vec{t}$ according to lexicographical ordering. The projections R_ϕ's are also serialized into one vector in following way:

$$\vec{r} = (\vec{r}_1, \vec{r}_2, \ldots, \vec{r}_\Phi) = (R_{1,1}, \ldots, R_{m,1}, \cdots, R_{1,\Phi}, \ldots, R_{m,\Phi})^\top \in \mathbb{R}^{m\Phi}$$

Each $\vec{r}_\phi$ is the lexicographical ordering vector of the projection ϕ. And m is the number of observed intensities in each projection image.

The task of algebraic image reconstruction is to solve the equation system

$$\mathbf{A}\vec{t} = \vec{r} \tag{6}$$

where the $(m\Phi \times N)$-matrix $\mathbf{A} = (a_{i,j})$ defines the projection geometry of a C-arm system or CT-scanner. Each $a_{i,j}$ element represents the contribution of the *j*th voxel to the *i*th ray during the casting of an X-ray through the human body. Several projection models are proposed by literature to determine the $a_{i,j}$ coefficients [15], [19]. In this work we employ the fast *alpha-clipping* algorithm [16]. Theoretically those more sophisticated projector models can also be used in this framework.

Many efficient algorithms are proposed for this large, sparse and unstructured problem. An excellent survey of these algorithms is given in [18]. In these reconstruction techniques, the 3D image $\vec{t}$ is usually initialized with zeros. In each iteration, every voxel has an individual relaxation residual that updates its intensity value. The reconstruction process stops when

$$\|A\vec{t}^{\,k} - \vec{r}\| < \epsilon. \tag{7}$$

The relaxation can be seen as a driving force in the reconstruction, whose value indicate scale signed "distances" between 3D image and observed projections. Ideally, when the observed 2D images are exactly the projections of the volume, the residuals on every voxels vanish. This strike property inspires us to use residuals to build up the external force for the 2D-3D registration equation.

3.2 2D-3D Distance using Mean Relaxation

In this work we use Censor and Gordon's component averaging (CAV) technique [14] to define the signed distance $D_u^R \in \mathbb{R}^3$. For the *j*th voxel, it is defined as

$$D_j^R(x, u(x)) = \frac{\lambda}{\Phi} \sum_{\phi=1}^{\Phi} \sum_{i=1}^{m} a_{i,j}^\phi \frac{r_{i,\phi}(x) - \langle \vec{a}^{i,\phi}, \vec{t}(x - u(x)) \rangle}{\sum_{l=1}^{n} s_l^\phi |a_{i,l}^\phi|^2}. \tag{8}$$

where $a^{i,\phi}$ is the *i*th row of $\mathbf{A}^\phi$ whereas $\mathbf{A}^\phi$ only contains the rays from projection ϕ, s_l^ϕ the number of non-zero elements in the *l*th column of $\mathbf{A}^\phi$ and $\lambda \in \mathbb{R}$ is a relaxation factor. The 2D residual $e_{i,\phi}^R := r_{i,\phi}(x) - \langle \vec{a}^{i,\phi}, \vec{t}(x - u(x)) \rangle$ between the projection of the deformed template and the observed reference image is averaged by the components $(a_{i,j})$ and back projected into 3D. D_u^R is then the mean relaxation (distance) between $\vec{t}$ and $\vec{r}$ for all given reference images. The convergence of the voxel relaxation in the CAV guarantees that D_u^R is bounded value [17]. Thus the new *relaxation force* $f^R \in \mathbb{R}^3$ is defined as

$$f^R(x, u(x)) = D_u^R \cdot \nabla T(x - u(x)). \tag{9}$$

The modified Euler–Lagrange equation becomes

$$f^R(x, u(x)) + \alpha \Delta^2[u](x) = 0. \tag{10}$$

With such relaxation force term, this equation characterizes the optimal 3D displacement field that minimizes the relaxation distance. At same time, it has same form with the original Euler–lagrange equation of 3D-3D registration problem. Thus we apply the same scheme in [12] to solve the equation (10). The non–rigid 2D-3D registration algorithm is summarized as following.

Algorithm 1 Nonrigid 2D-3D registration

%Initialization
$u^{(k)} = 0$.
for $k = 0, 1, ...$ **do**
  Compute $D^{R,(k)}(x, u(x))$ using (8)
  Compute $f^{R,(k)}$ using (9).
  Compute $u^{(k+1)}$ via solving Eq (10).
end for

4 Experiments

Experimental results are presented on artificial 2D-3D phantoms and real 3D DSA data. For the experiments we resampled all volume data to $64 \times 64 \times 64$ and the projection images to 128×128. The projection geometry for each X-ray image is given from a real C-arm system. This projection geometry has been estimated in a calibration step. We use only monomodal image data in our experiments.

The *relative error* $\epsilon^{(k)}$ between the ground truth template image T^{GT} and the deformed template image $T(x - u(x)$ is defined as

$$\epsilon^{(k)} := \frac{1}{\sum_{j=1}^{N} |T_j^{GT}|} \sum_{j=1}^{N} |T_j^{(k)}(x - u(x)) - T_j^{GT}| \tag{11}$$

and the 2D-3D distance $\tilde{D}$ with

$$\tilde{D}^{(k)} := \frac{1}{N} \sum_{j=1}^{N} (D_j^R(x, u(x)))^2 \tag{12}$$

4.1 Phantom

We first evaluate the 2D-3D registration on a sphere-cube phantom as shown in fig. 2, 1. We register a 3D cube with *digitally reconstructed radiographs* (DRRs) from a sphere. For practical application it is important to show that it works also with a very sparse number of projection images. Figure 3 shows the relationship between the 2D-3D relaxation distance and the number of projection images.

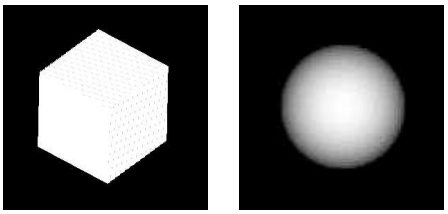

3D-cube 2D-sphere projection

Figure 1: 3D-cube/2D-sphere phantom

We can verify on the phantom data (fig. 2) that even for $\Phi = 2, 3$ reference images the computed deformation field (fig. 2) is smooth and the cube is deformed into a sphere (fig. 4). The deformation field using $\Phi = 3$ reference images is more precise than the one using only $\Phi = 2$ (approximately orthogonal) projections. The relaxation distance (fig. 3) for $\Phi = 6$ reference images (unique distributed projection angle) is also smoother and a more representative dissimilarity than the one computed with $\Phi = 2$ projections. Both the relative error $\epsilon^{(k)}$ and $\tilde{D}^{(k)}$ decrease with an increasing number of iterations (fig. 5, 6). In conclusion we can say that for $\Phi = 4, 3$ and even 2 projections we got an impressive match of the 3D cube and the sphere projections.

4.2 Medical Data

To evaluate the 3D deformation field using medical data we use a real 3D DSA image that was reconstructed via *Filtered Backprojection* and add a nonrigid deformation. The image contains with contrast agent filled vessels (white). Thus we do not have real fluoroscopic images we compute the DRRs from the vessel image before the 3D-deformation and register afterwards the synthetic deformed DSA image with the DRRs. The result is shown and discussed in fig. 9, 10, 8 and 7.

5 Discussion

5.1 2D-3D Distance

The quality of the 2D-3D distance depends on Φ, the number of reference images used for the D_u^R

computation and the corresponding projection angle distribution of the reference images. Obviously a uniform distribution of the projections over 180 degree around the body will provide a better distance meassure than a non-uniform and limited angle distribution. However could we even achieve promising results with phantom data using only two approximately orthogonal aligned reference images. To achieve satisfactory results with real data more than two projections are required. In practice can the registration start with two projections and additional acquired projections during the intervention can be added sequencially.

5.2 Projector Model

The *alpha-clipping* projector model we used in our experiments is fast, but also one of the simplest one that introduce artifacts to the projection. These artifacts affect the quality of the relaxation distance in a negative manner. This can be improved by using a more sophisticated projector model [15]. Reconstruction artifacts in the pre-reconstructed template image may also cause problems, depending on the strength of these artifacts. The relaxation distance depends also on the residuals $e^R_{i,\phi}$ of the computed volume projections and the acquired projection images from the physical X-ray scanner. Here we suggest applying a denoising of noisy low contrast fluoroscopic images before computing the relaxation distance.

5.3 Image Modality

The current approach is limited to monomodal registration, but reformulating the iterative algebraic reconstruction to a statistical representation [18] - maximum likelihood algorithms (RAMLA) - the relaxation distance may extended to a multi-modal registration scheme.

6 Summary

The 2D-3D registration problem can be classified into two *problem models*:

1. Projection of the 3D template $\mathbf{A}\vec{t}$ and computing the 2D-3D distance and deformation field in 2D.
2. Backprojection of 2D residuals by inversion of $\mathbf{A}^\dagger\vec{r}$ into 3D and computation of a 3D distance and deformation field.

In this paper we address the second problem model. We use Censor and Gordon's CAV reconstruction technique to backproject the 2D dissimilarity into 3D. The substitution of the mono-dimensional force term (5) with a 2D-3D force term (9) allows to deal with the non-rigid 2D-3D registration problem like a 3D-3D registration. A large benefit of this technique is the usability of well studied existing non-rigid 3D-3D registration approaches.

References

[1] Gueziec, A., "*Assessing the registration of CT-scan data to intraoperative x-rays by fusing x-rays and preoperative information*", *Proceding SPIE Medical Imaging'99*, p. 3661-3688.

[2] Feldmar, J., N. Ayache and F. Betting, "*3D-2D projective registration of free–from curves and surfaces*", 1994, INRIA, France.

[3] Hamadeh, A., et al., "*Towards automatic registration between CT and X-ray images: cooperation between 3D/2D registration and 2D edge detection*", in 2nd Annual Internaltional Symposium on MRCAS, 1995. Baltimore, MD USA.

[4] Weese, J., et al. "*An Approach to 2D/3D Registration of a Vertebra in 2D X-ray Fluoroscopes with 3D CT Images*", in Computer Vision and Virtual Reality in Medicine II - Medical Robotics and Computer Assisted Surgery III, 1997, France.

[5] LaRose, D., "*Iterative X-ray/CT registration using accelerated volume rendering*", in Robotics Institute, 2001, Carnegie Mellon University.

[6] Zollei, L., "*2D-3D rigid registration of X-ray fluoroscopy and CT images using mutual information and sparsely sampled histogram estimators*", in IEEE CVPR, 2001.

[7] Yao, J., et al. "*Assessing accuracy factors in deformable 2D/3D medical image registration using a statistical Pelvis model*", in Proceedings of the Ninth IEEE International Conference on Computer Vision (ICCV 2003) 2-Volume.

[8] Broit, C. *Optimal registration of deformed images*, Ph.D Thesis, Computer and Information Science, Uni Pensylvania, 1981.

[9] Morten, B., *Medical image registration and surgery simulation*, Ph.D Thesis, IMM, Tech-

nical University of Denmark, 1996.

[10] Christensen, G., *Deformable shape models for anatomy*, Ph.D Thesis, Sever Institute of Technology, Washington University, 1994.

[11] Fischer, B. and Modersitzki, J. *Fast diffustion registration*, AMS contemporary Mathematics, Inverse Problems, Image Analysis, and Medical Imaging, vol. 313, 2002, pp: 117-129.

[12] Fisher. B and J. Modersitzki, "*Curvature based image registration*", JMIV 18(1), 2003.

[13] Y. Censor and T. Elfving, "*Block-Iterative Algorithms with Diagonally Scaled Oblique Projections for the Linear Feasibility Problem*", SIAM Journal on Matrix Analysis and Applications, vol. 24, number 1, p. 40-58, 2002.

[14] Y. Censor and D. Gordon and R. Gordon, "*Component averaging: An efficient iterative parallel algorithm for large and sparse unstructured problems*", Parallel Computing, vol. 27, pp. 777-808, 2001.

[15] K. Mueller and R. Yagel and J. J. Wheller, "*Fast Implementation of Algebraic Methods for 3D Reconstruction from Cone-Beam Data*", IEEE Trans. Med. Imaging, Vol. 18, No. 6, pp. 538-548, 1999.

[16] J. D. Foley and A. van Dam and S. K. Feiner and J. F. Hughes, "*Computer Graphics: Principles and Practice in C*", isbn 0201848406, 1995, Addison-Wesley Professional.

[17] M .Jiang, G. Wang, "*Convergence studies on iterative algorithms for image reconstruction*", IEEE Trans Med Imaging. 2003 May, Vol. 22 No. 5, pp. 569-79.

[18] M .Jiang, G. Wang, "*Development of iterative algorithms for image reconstruction*", Journal of X-Ray Science and Technology Vol. 10, 2002, pp. 77-86, IOS Press.

[19] P. E. Danielsson and M. Magnusson Seger "*Combining Fourier and iterative methods in computer tomography. Analysis of an iteration scheme. The 2D-case*", Dept. EE, Linköping University, Oct. 2004, No. LiTH-ISY-R-2634, SE-581 83 Linköping, Sweden.

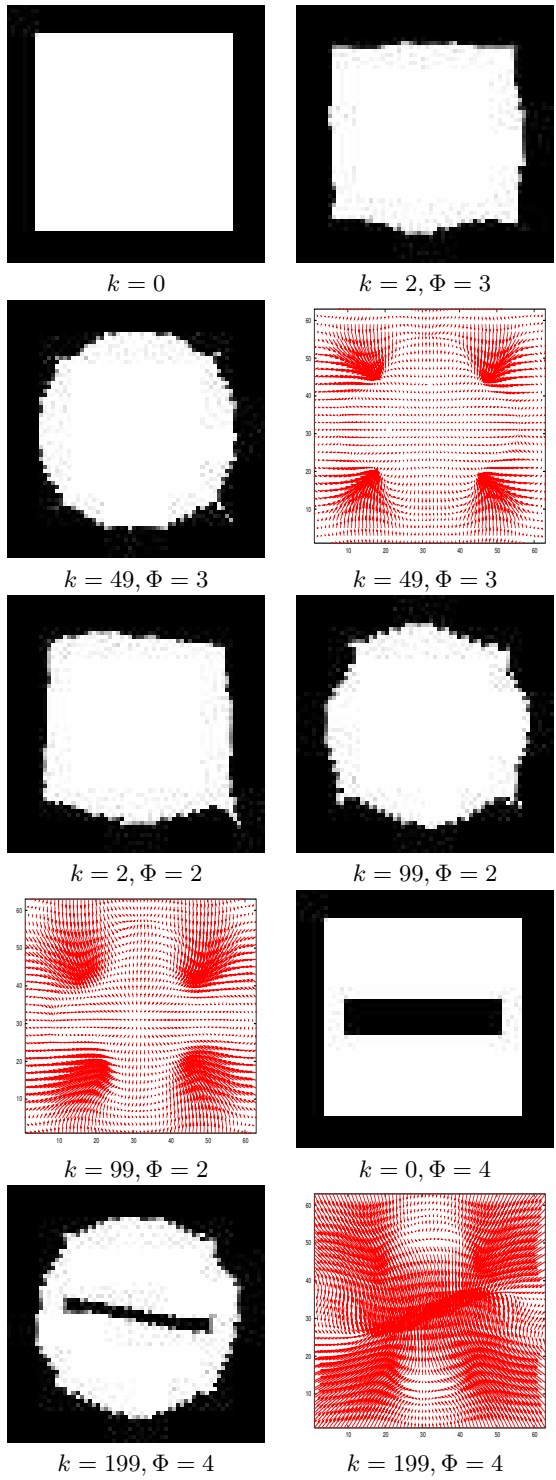

Figure 2: 3D-2D cube-sphere registration after k iterations ($\lambda = 1.5, \tau = 2, \alpha = 5$, center volume slice of deformed 3D-template).

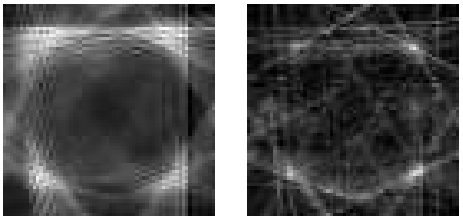

$k = 0, \Phi = 6$ $k = 69, \Phi = 6$

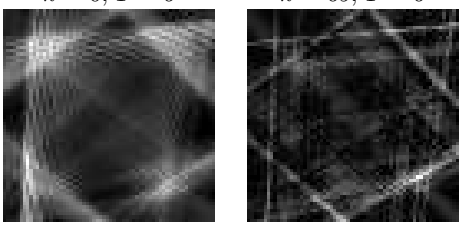

$k = 0, \Phi = 4$ $k = 49, \Phi = 4$

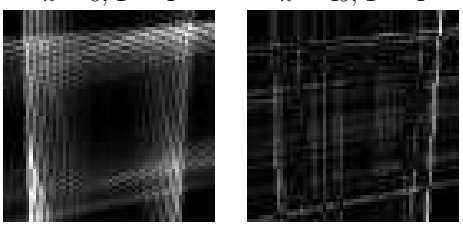

$k = 0, \Phi = 2$ $k = 99, \Phi = 2$

Figure 3: 3D-2D cube-sphere relaxation distance $D^R(x, u(x))$ after k iterations ($\lambda = 1.5,\ \tau = 2,\ \alpha = 5$, center volume slice).

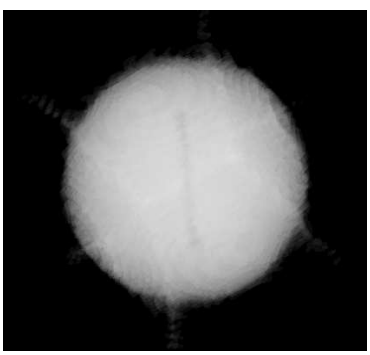

Figure 4: Rendered 3D-cube template (cube with small rectangular hole inside; see fig. 2) after registration with 2D-sphere projections. The rectangular hole is almost closed inside the defomed cube ($k = 99,\ \Phi = 4,\ \lambda = 1.5,\ \tau = 2,\ \alpha = 5$).

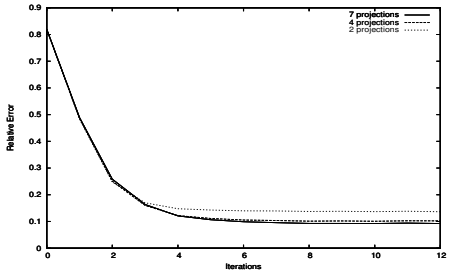

Figure 5: Relative error $\epsilon^{(k)}$ (11) between T^{GT} and $T^{(k)}(x - u(x))$.

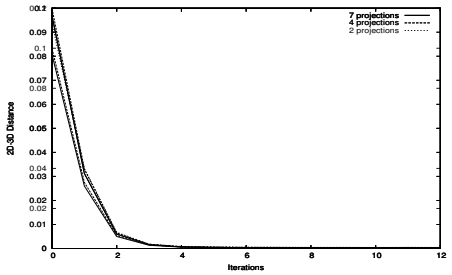

Figure 6: 2D-3D distance $\tilde{D}^{(k)}$ (12) after k iterations ($\lambda = 1.5,\ \tau = 2,\ \alpha = 5$).

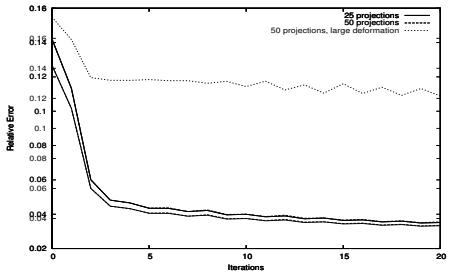

Figure 7: Relative error $\epsilon^{(k)}$ (11) between T^{GT} and $T^{(k)}(x - u(x))$.

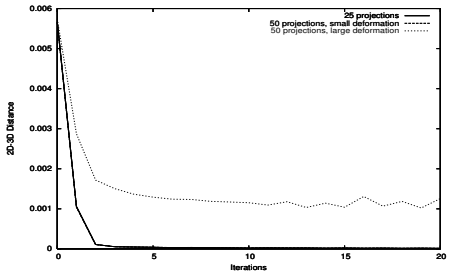

Figure 8: 2D-3D distance $\tilde{D}^{(k)}$ (12) after k iterations ($\lambda = 1.5,\ \tau = 2,\ \alpha = 5$).

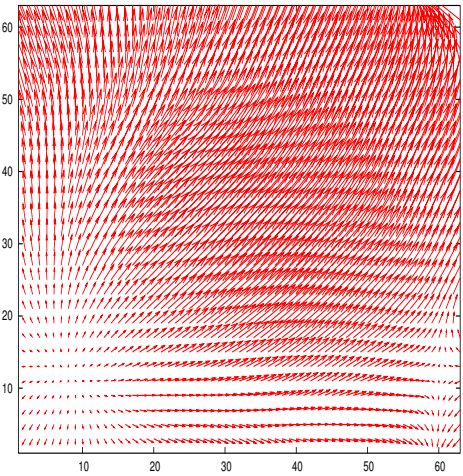

$k = 199, \Phi = 50$

$k = 199, \Phi = 50$

Figure 9: **Top:** orthogonal projection of the deformation field $u(x)$ of the center volume slice. **Bottom:** difference image $T^{GT} - T(x - u(x))$. The non-rigid deformation between the reference and template is about five voxel in diagonal volume direction ($\lambda = 1.5, \tau = 25, \alpha = 5$). The computed deformation field represents the synthetic applied non-rigid diagonal deformation direction.

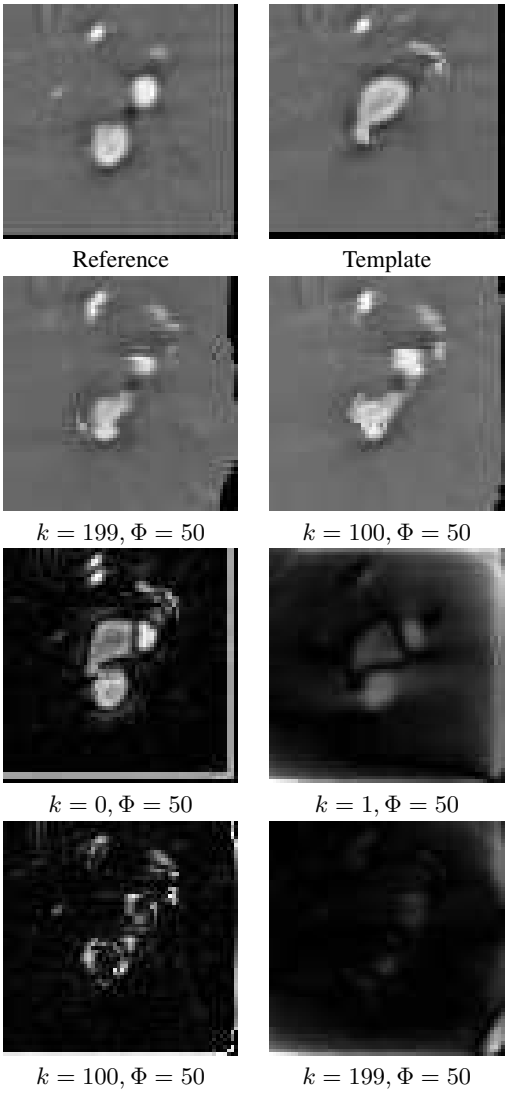

Figure 10: **Top:** reference and template center volume slice (cvs). The added non-rigid deformation is about six voxel in diagonal volume direction. The two vessels appear merged in the cvs because there is a branch. **2nd row:** after registration are the vessels moved back such that both vessels are shown seperately in the cvs. **3nd row:** difference image (left) and D_u^R of cvs (right). **Bottom:** difference image and D_u^R after k iterations ($\lambda = 1.5, \tau = 25, \alpha = 5$).